

EQ-Net: A Unified Deep Learning Framework for Log-Likelihood Ratio Estimation and Quantization

Marius Arvinte, Ahmed H. Tewfik, and Sriram Vishwanath

Abstract

In this work, we introduce EQ-Net: the first holistic framework that solves both the tasks of log-likelihood ratio (LLR) estimation and quantization using a data-driven method. We motivate our approach with theoretical insights on two practical estimation algorithms at the ends of the complexity spectrum and reveal a connection between the complexity of an algorithm and the information bottleneck method: simpler algorithms admit smaller bottlenecks when representing their solution. This motivates us to propose a two-stage algorithm that uses LLR compression as a *pretext* task for estimation and is focused on low-latency, high-performance implementations via deep neural networks. We carry out extensive experimental evaluation and demonstrate that our single architecture achieves state-of-the-art results on *both* tasks when compared to previous methods, with gains in quantization efficiency as high as 20% and reduced estimation latency by up to 60% when measured on general purpose and graphical processing units (GPU). In particular, our approach reduces the GPU inference latency by more than two times in several multiple-input multiple-output (MIMO) configurations. Finally, we demonstrate that our scheme is robust to distributional shifts and retains a significant part of its performance when evaluated on 5G channel models, as well as channel estimation errors.

I. INTRODUCTION

Recent years have seen deep learning methods mature and become more pervasive in communication networks research [1]. At the center of our goal and methods are two of the core tasks of any digital system: estimation and quantization. High-performance solutions for these two tasks are critical for the functioning of any in-the-wild digital communication system. Furthermore, algorithms developed at the intersection of deep learning and digital communications are faced with the unique challenges of timing and power constraints [2]. For example, energy and memory efficient quantization is critical in distributed systems [3], where information is often sent through

relays or stored for mid-term usage (e.g., hybrid retransmission requests). At the same time, without efficient estimation algorithms applicable in high-dimensional scenarios, the end-to-end communication link can suffer an unwanted increase in latency or drop in performance.

In this work, we introduce EQ-Net — the first deep learning framework that jointly tackles both log-likelihood ratio estimation and quantization using a shared feature space. Our work is motivated by the information bottleneck method [4], [5] and its applicability to the task of MIMO detection. To achieve this, we first prove that two of the most well-known MIMO detection algorithms also perform *implicit* compression: the solutions output by these algorithms admit exact lower-dimensional representations, with less complex (and worse performing) algorithms compressing more. Motivated by this, EQ-Net is a data-driven algorithm that learns a compressed, low-dimensional representation of the optimal solution *and* retains high estimation performance. The practical implementation of our algorithm is achieved with a low-latency, *non-iterative* and *non-model-based* deep learning architecture that uses compression as a *pretext* task for learning an estimation function in a two-stage training protocol.

Log-likelihood ratio estimation has been extensively investigated using classical methods, and more recently, using data-based approaches as well. One of the first modern algorithms for MIMO detection is V-BLAST [6], which introduces the idea of sequential estimation. Soft-output sphere decoding [7] generalizes this approach and is one of the most high-performing algorithms with sub-exponential complexity, however its practical end-to-end latency is still prohibitive even for moderately-sized systems due to its sequential nature. More recently, the work in [8] proposes OAMP-Net2 as a data-based extension to the OAMP detection algorithm [9], where the step sizes are treated as learnable parameters. The work in [10] takes a similar approach, but replaces the fixed computations of the OAMP algorithm with fully learnable transforms, resulting in state-of-the-art results for LLR estimation. Similarly, the authors in [11] propose an architecture suitable for integration in the Viterbi decoding algorithm that also blends learnable transforms with classical algorithms.

More generally, previous methods involve the idea of unrolled optimization and model-based learning. In contrast, our proposed approach is orthogonal to these ideas and solves MIMO detection *without* any recurrency or unrolling, leading to low-latency solutions. A different type of approach is the work in [12], where a two-layer neural network learns a piecewise linear approximation of the log-likelihood ratios in AWGN channels. However, as our ablation experiment shows, learning a good solution for the MIMO detection problem is much more

difficult with plain (black-box) end-to-end learning.

Concerning quantization, the work in [13] introduces an information-theoretic optimal data-based approach for quantizing log-likelihood values that are drawn from the same distribution (e.g., corresponding to bits found at the same position in Gray-coded digital quadrature amplitude modulation).

The deep learning approach in [14] leverages the redundancy between LLR values corresponding to the channel use and achieves state-of-the-art quantization results for scalar channels. This work is inspired by [14], with the following important distinctions: (i) EQ-Net is designed for and applicable to general MIMO channels, and we perform experiments showing that naively extending [14] suffers a performance loss, (ii) the previous approach is not suitable for out-of-the-box estimation, whereas EQ-Net is designed from the ground-up for both tasks, and (iii) EQ-Net introduces a novel two-stage training scheme and a residual architecture for the estimation encoder.

To quantify the benefits of our approach, we perform end-to-end simulations in several MIMO channel configurations and compare against state-of-the-art methods. We also evaluate the system latency of our approach on both general purpose (CPU) and graphical processing units (GPU) and demonstrate that we can achieve near sub-millisecond latency while significantly improving end-to-end performance against the baselines. Finally, we also evaluate the robustness of our estimator when faced against distributional shifts and imperfections in channel knowledge.

Summarized, our contributions are:

- 1) We prove that two of the most well-known MIMO detection algorithms perform implicit compression.
- 2) We introduce EQ-Net, a deep learning approach that jointly solves the tasks of LLR estimation and quantization for MIMO communication systems.
- 3) We perform extensive experimental evaluations that validate our design choices and show state-of-the-art performance on both tasks simultaneously.

II. SYSTEM MODEL

We assume a narrowband, instantaneous digital communication model given by (1). This encompasses several of the most practical scenarios, such as single carrier communication or an individual subcarrier of a MIMO-OFDM transmission, and is flexible enough to model various distributions of \mathbf{H} :

$$\mathbf{y} = \mathbf{H}\mathbf{x} + \mathbf{n}, \quad (1)$$

where $\mathbf{x} \in \mathbb{C}^{N_t}$ is a vector of transmitted symbols and $\mathbf{y} \in \mathbb{C}^{N_r}$ is a vector of received symbols. N_t and N_r represent the number of transmitted and received symbols, respectively. $\mathbf{n} \in \mathbb{C}^{N_r}$ is an i.i.d. complex Gaussian noise vector with covariance matrix $\sigma_n^2 \mathbf{I}$. We assume that transmitted symbols are uniformly drawn from the discrete constellation \mathcal{C} containing a number of 2^K complex symbols. \mathbf{H} is the equivalent digital channel matrix between the transmitter and receiver and already includes any potential precoding or beamforming. We call K the modulation order.

Given channel knowledge (or an estimate of \mathbf{H}) and the received vector \mathbf{y} , the exact log-likelihood ratio (LLR) for the i -th bit of the k -th transmitted symbol is defined as

$$\Lambda_{i,k} = \log \frac{\sum_{\mathbf{x} \in \mathcal{C}, b_{k,i}=1} \exp -\frac{\|\mathbf{y}-\mathbf{H}\mathbf{x}\|_2^2}{\sigma_n^2}}{\sum_{\mathbf{x} \in \mathcal{C}, b_{k,i}=0} \exp -\frac{\|\mathbf{y}-\mathbf{H}\mathbf{x}\|_2^2}{\sigma_n^2}}. \quad (2)$$

Equation (2) is the maximum likelihood (ML) solution to the LLR estimation problem, under the assumption that \mathbf{n} is i.i.d. Gaussian. The sums in (2) involve a number of $2^{KN_t}/2$ terms for both the denominator and the numerator, leading to a prohibitive computational complexity at inference time even for moderate values of N_t and K . It is thus a sensible choice to adopt a data-based approach and amortize this complexity during training, with the hope of obtaining a low-latency inference mechanism (e.g., a lightweight neural network).

Given the QR decomposition of $\mathbf{H} = \mathbf{Q}\mathbf{R}$ and exploiting the fact that \mathbf{Q} is always a matrix with orthonormal columns and satisfies $\|\mathbf{Q}\mathbf{x}\|_2 = \|\mathbf{x}\|_2$ for any complex vector \mathbf{x} , (2) can be rewritten as

$$\Lambda_{i,k} = \log \frac{\sum_{\mathbf{x} \in \mathcal{C}, b_{k,i}=1} \exp -\frac{\|\hat{\mathbf{y}}-\mathbf{R}\mathbf{x}\|_2^2}{\sigma_n^2}}{\sum_{\mathbf{x} \in \mathcal{C}, b_{k,i}=0} \exp -\frac{\|\hat{\mathbf{y}}-\mathbf{R}\mathbf{x}\|_2^2}{\sigma_n^2}}, \quad (3)$$

where $\hat{\mathbf{y}} = \mathbf{Q}^H \mathbf{y}$. The upper triangular structure of \mathbf{R} can be exploited for an efficient implementation of the zero-forcing successive interference cancellation (ZF-SIC) detection algorithm [15], where detection starts from the N_t -th stream and proceeds upwards, as briefly described in Algorithm 1.

Algorithm 1: ZF-SIC Detection via QR Decomposition.

Input: $\hat{\mathbf{y}}, \mathbf{R}, \mathcal{C}$
for $k = N_t : 1 : -1$ **do**

Subtract previous interference

$$\tilde{\mathbf{y}}_k = \hat{\mathbf{y}}_k - \sum_{j=N_t}^{k+1} r_{k,j} \tilde{\mathbf{x}}_j$$

Compute LLR by marginalization

$$\Lambda_{i,k} = \log \frac{\sum_{x_j \in \mathcal{C}, b=1} \exp -|\tilde{y}_k - r_{k,k} x_j|^2}{\sum_{x_j \in \mathcal{C}, b=0} \exp -|\tilde{y}_k - r_{k,k} x_j|^2}$$

Update hard estimate

$$\tilde{x}_k = \arg \min_{x_j \in \mathcal{C}} |\tilde{y}_k - r_{k,k} x_j|^2$$

end for
Output: $\Lambda_{\text{ZF-SIC}} \leftarrow \Lambda$

Throughout the paper, we target the tasks of quantization and estimation of the LLR vector corresponding to a single channel use (i.e., one instance of (1)). Even though our proposed approach is applied independently to each channel use for both tasks, we evaluate end-to-end performance under a block coding scenario, where bits are shuffled, aggregated in codewords and transmitted over multiple channel uses, as is considered standard practice [16]. This setting is applicable both to the receiver of a downlink channel — a user terminal or an intermediate relay in distributed communications — and the receiver of an uplink channel — a base station that simultaneously receives data from a large number of distributed users.

III. COMPRESSED REPRESENTATIONS OF ESTIMATED LLR VECTORS

To motivate our proposed deep learning approach, we introduce and prove two theorems concerning the induced structure of the solutions of two canonical log-likelihood ratio estimation algorithms. Intuitively, the main takeaway of this section is that sub-optimal soft-output estimation algorithms output a solution vector which can be losslessly compressed to a size smaller than that of the optimal solution.

Recognizing that there is a large performance gap incurred by simple, conventional algorithms (i.e., with sub-exponential complexity), we posit that a data-driven approach can cover this gap and discover a low-complexity, high-performance estimation algorithm that also compresses the returned solution.

A. Compressed Representation of ZF-SIC Solution

To begin, we consider the soft-output version of the ZF-SIC algorithm given by Algorithm 1. Given channel knowledge \mathbf{H} , the algorithm sequentially estimates transmitted symbols x_i by leveraging the QR decomposition of \mathbf{H} . Once a symbol is estimated, it is subtracted from all other received streams and detection continues. Note that for the purposes of our theorem we do not assume any specific channel ordering, such as the one used in V-BLAST [6] and its extensions.

Theorem 1 (Dimension of ZF-SIC Solution): Let $\mathbf{\Lambda}_{\text{ZF-SIC}} \in \mathbb{R}^{KN_t}$ be the solution obtained by the ZF-SIC algorithm. Then, there exists a surjective function $g : \mathbb{R}^{d_{\text{ZF-SIC}}} \mapsto \mathbb{R}^{KN_t}$, such that:

$$g(\mathbf{z}) = \mathbf{\Lambda}_{\text{ZF-SIC}},$$

where

$$d_{\text{ZF-SIC}} = 3N_t,$$

for all modulation orders K .

Proof: See Appendix A. ■

Theorem 1 states that any vector solution obtained by the ZF-SIC algorithm admits an *exact* low-dimensional representation. Intuitively, this result can be made apparent by noting that the ZF-SIC algorithm effectively approximates the \mathbf{R} matrix with its diagonalized version. In this case, all symbols are decoupled and the set of LLR values corresponding to a specific transmitted stream can be exactly stored using *three* values. This leads to a total of $3 \times N_t$ real values required to store the entire $\mathbf{\Lambda}$ vector. For a single-input scenario, this is the basis for the prior work in [14], where the vector of LLR values is compressed to a dimension of three, regardless of modulation size in a single-input single-output scenario. For the purpose of our work, Theorem 1 extends this to the solution output by the ZF-SIC estimation algorithm in a MIMO scenario.

B. Compressed Representation of ML Solution

We move towards the opposite end of the spectrum of estimation algorithms and consider optimal MIMO detection. Given channel knowledge, ML can be cast an exhaustive tree search algorithm across all possible sets of transmitted symbols that aggregates their contributions to estimate the soft outputs. We consider the exact implementation of (2), whose time complexity scales exponentially with the number of transmitted streams N_t .

Theorem 2 (Dimension of ML Solution): Let $\mathbf{\Lambda}_{\text{ML}} \in \mathbb{R}^{KN_t}$ be the solution obtained by the ML algorithm. Then, there exists a surjective function $g : \mathbb{R}^{d_{\text{ML}}} \mapsto \mathbb{R}^{KN_t}$ such that:

$$g(\mathbf{z}) = \mathbf{\Lambda}_{\text{ML}},$$

where,

$$d_{\text{ML}} = N_t(N_t + 2),$$

for all modulation orders K .

Proof: See Appendix B. ■

Theorems 1 and 2 inform us that $d_{\text{ZF-SIC}} = 3 \times N_t$ and $d_{\text{ML}} = N_t \times (N_t + 2)$, respectively, leading to the straightforward deduction that

$$d_{\text{ZF-SIC}} < d_{\text{ML}}, \quad \forall N_t > 1. \quad (4)$$

Note that since there are a total KN_t LLR values corresponding to a single channel use, the compression ratios of ZF-SIC and ML are

$$\begin{aligned} R_{\text{ZF-SIC}} &= \frac{KN_t}{d_{\text{ZF-SIC}}} = \frac{K}{3}, \text{ and,} \\ R_{\text{ML}} &= \frac{KN_t}{d_{\text{ML}}} = \frac{K}{N_t + 2}, \end{aligned} \quad (5)$$

respectively.

If $K \geq 3$, then the solution of ZF-SIC *always* admits a compressed representation, while the required condition for ML is more stringent and takes the form $K \geq N_t + 2$. This offers a novel perspective on soft estimation algorithms based on the compression ratio R : instead of the well-known complexity vs. performance trade-off, the maximal lossless compression of the obtained solution is also an aspect that appears when analysing an algorithm. The simple (in terms of computational complexity) ZF-SIC method can be interpreted as finding an implicitly compressed estimate of the ML solution, which in turn helps alleviate computational complexity through the low-dimensional assumption.

These observations motivate our deep learning-based architecture as a feature learning algorithm with a compressed feature representation of size equal to that of the ZF-SIC solution. We conjecture that there exist other algorithms that, while not interpretable, outperform ZF-SIC significantly when mapping the solution to a feature space of the same size. These learnable algorithms thus serve as an application of the information bottleneck [4] principle to MIMO

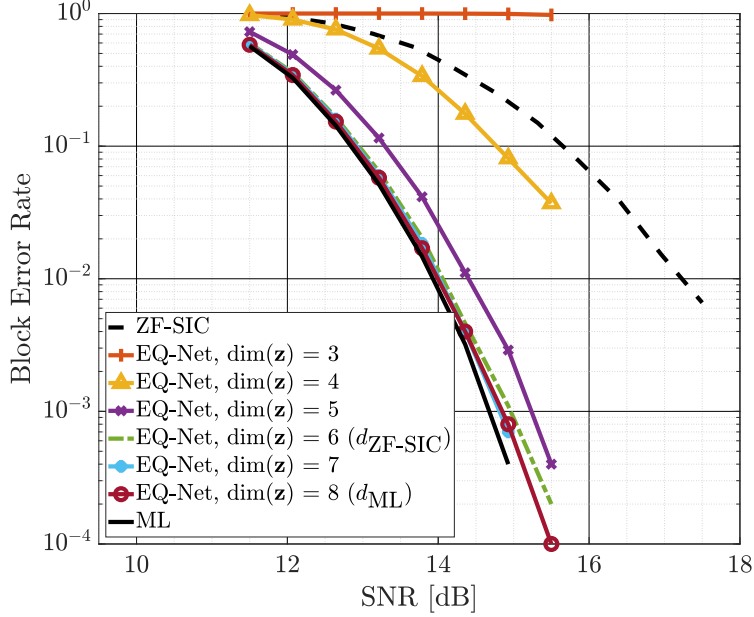


Fig. 1. Compression performance of different instances of EQ-Net and the two reference algorithms without any numerical quantization in an i.i.d. Rayleigh fading, 2×2 64-QAM scenario with an $(324, 648)$ LDPC code. A bottleneck size of six corresponds to the implicit dimension of the ZF-SIC solution (Theorem 1), but retains near-ML performance.

detection: the compressed representation would serve as an efficient estimator, given that we can successfully train an estimation encoder that maps directly from the received sample to it.

Since such an algorithm does not have a closed-form expression, we resort to a data-driven approach for learning a model which approximates this optimal algorithm (according to information bottleneck principles) in terms of end-to-end performance.

C. Impact of Bottleneck Size

To verify Theorems 1 and 2, and our conjecture, we train a sequence of compressive autoencoders, where the only parameter that changes is the bottleneck size (we also use the notion of latent space dimension interchangeably). For exemplification, we target a 2-by-2, 64-QAM scenario under i.i.d. Rayleigh fading, but this result holds for arbitrary configurations. For this scenario, we have that:

$$\begin{aligned} d_{\text{ZF-SIC}} &= 6, \\ d_{\text{ML}} &= 8. \end{aligned} \tag{6}$$

Theorems 1 and 2 inform us that the simplest possible (and with the worst non-trivial performance) algorithm, ZF-SIC, implicitly projects the log-likelihood ratio vector onto a *six-*

dimensional manifold and that the ML solution lies on an *eight*-dimensional manifold. Our conjecture is that there exist learnable algorithms that project onto a lower-dimensional feature space than ML, but still retain most of its performance.

Fig. 1 plots the end-to-end performance when the bottleneck size is the only parameter that is varied. In all cases, the LLR vector is estimated with the optimal ML algorithm and is then lossy compressed, but not numerically quantized. For reference, we also plot the two conventional ZF-SIC and ML algorithms with latent spaces of size $d_{\text{ZF-SIC}} = 6$ and $d_{\text{ML}} = 8$, respectively. Two conclusions can be drawn from this plot:

- 1) A purely data-based approach *can* find nonlinear low-dimensional projections that greatly improve the performance compared to the ZF-SIC algorithm, and retain the same compression ratio.
- 2) Any attempt to further compress the optimal LLR vector is met with an increase of error and departure from ML performance, but can still outperform ZF-SIC estimation. This hints at the possibility of learning data-based approaches with a sub-linear (w.r.t. the number of transmitted data streams) dimension of the solution manifold.

For the rest of this work, we use a latent space with $\dim(\mathbf{z}) = 3N_t$ — the same as the ZF-SIC algorithm — due to the minimal performance loss incurred and to compress as much as possible. This has the benefit of a linearly increasing compression gain as modulation size increases. While the second observation could be used to further compress the vector of log-likelihood ratios in higher-dimensional MIMO transmissions, where the performance/complexity gap between ML and ZF-SIC increases, our results are targeted at digital communication scenarios with $N_t \leq 4$ and an increased modulation size.

While the size of the compressed representation is positively correlated with the computational complexity of both algorithms, we note that there are two important distinctions between bottleneck (compressed) dimension and complexity:

- 1) The former increases quadratically when moving the ZF-SIC to the optimal ML solution, while the computational complexity suffers an exponential increase.
- 2) The size of the compressed representation is *independent* of the modulation size for both algorithms, while the complexity suffers an exponential increase for the ML solution. This motivates data-based approaches, particularly in regimes where a high modulation order is used leading to a *free* compression gain.

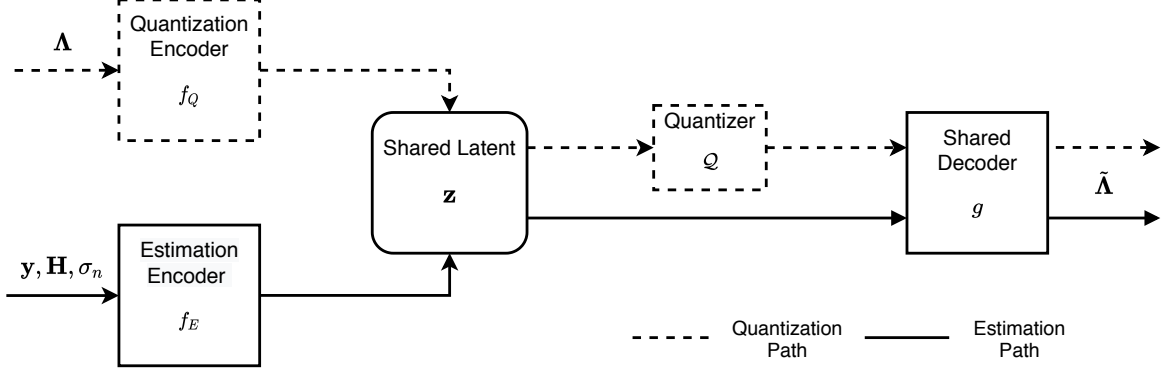


Fig. 2. High-level block diagram of the proposed architecture. The two encoders and the shared decoder are implemented as deep neural networks with a small number of hidden layers to ensure a low-latency signal path. The dotted lines indicate all components trained in the first stage and can be used for quantization at test time. The estimation encoder f_E is trained *after* the first stage, with all other components frozen.

The two properties endow EQ-Net with the following concurrent interpretations:

- EQ-Net is a compression algorithm that retains near-ML performance while mapping the vector of LLR values to a bottlenecked feature space of size $d_{\text{ZF-SIC}}$.
- EQ-Net is an estimation algorithm that encompasses ZF-SIC as a local minima in the loss landscape, but benefits from a sufficient number of trainable parameters to learn better solutions.

IV. EQ-NET: JOINT ESTIMATION AND QUANTIZATION

Our scheme uses lossy compression as a *pretext task* for estimation: when learning the estimator, we do not learn a direct mapping from symbols to the vector of LLR values, but rather split the learning in two conceptually separate stages. Our ablation experiments show that this is an essential step when training a model with limited depth and width and that single stage end-to-end training falls into unwanted local minima. Once a compression model is successfully trained, we apply a form of teacher-student training and directly map the pair formed by the received symbols and channel knowledge to its corresponding latent code. The architecture of EQ-Net is comprised of three functional blocks, with training carried out across two stages. A high-level functional block diagram is shown in Fig. 2.

A. Compression as Pretext Task for Estimation

In the first stage, we train an autoencoder composed from the quantization encoder f_Q and shared decoder g_Q . The input to the autoencoder is a vector of LLR values estimated with the ML algorithm or, when this is not feasible even at training time, with an approximate ML algorithm such as the soft-output sphere detection algorithm. The loss function used is the same as [14], namely the inter- and intra-LLR weighted mean squared error loss given by

$$L_q = \sum_{i=1}^K w_i \frac{\|g_Q \circ \mathcal{Q} \circ f_Q(\Lambda_i) - \Lambda_i\|_2^2}{|\Lambda_i| + \epsilon}. \quad (7)$$

Similarly to [14], we use a value of $\epsilon = 10^{-6}$ to stabilize the loss function around low-magnitude values. The weights w_i are proportional to the average magnitude of each LLR in the training dataset. The quantizer \mathcal{Q} is a function that maps the interval $[-1, 1]$ to a discrete and finite set of points \mathcal{C} with a resolution of N_b bits. During training, we replace the hard quantization operator with a differentiable approximation during training to obtain useful gradients. We follow our previous work [14] and use a simple Gaussian noise model during training as the operator

$$\mathcal{Q}_{train}(x) = x + u, \quad (8)$$

where u is drawn from $\mathcal{N}(0, \sigma_u)$ and $\sigma_u = 0.001$. To prevent the network from learning a trivial solution by amplifying the magnitude of the latent components, we use a hyperbolic tangent activation on the output layer of f_Q . When benchmarking the performance of the noise-based approach versus the commonly used straight-through estimator, we find that this choice of \mathcal{Q} exhibits better convergence properties and offers satisfactory test-time performance.

Once the autoencoder is trained we obtain the latent representation \mathbf{z} by passing all training samples through the encoder f_Q but not through the quantizer (or its differentiable approximation). We include \mathbf{z} as a separate functional block in Fig. 2 since it is useful to make the connection with the two theorems in the previous section: \mathbf{z} defines the geometry of the low-dimensional manifold our estimation algorithm will operate on. In this sense, our scheme leverages compression as a pretext task for learning a well-shaped, robust manifold of the data.

In the second stage, we train an estimation encoder f_E to map received samples and channel state information to the same latent code output by the quantization encoder, that is, to map directly on the manifold given by \mathbf{z} . As a latent loss we use the L1 distance, since we *a priori*

know that all valid latent codes are bounded by $(-1, 1)$. The supervised estimation training loss is given by

$$L_e = \|f_E(\mathbf{y}, \mathbf{H}, \sigma_n; \theta_e) - f_Q(\mathbf{\Lambda})\|_1. \quad (9)$$

Intuitively, the pair f_Q and f_E behaves exactly like a feature teacher-student pair [17] that performs knowledge distillation. Since we already have a good decoder in g , this allows us to give up the end-to-end reconstruction objective in the second stage and map received symbols to a static, pre-trained latent space. In our experiments, we show that this is critical for the convergence of shallow, low-latency networks to high performance solutions.

B. Operating Modes

At test time, given a set of received antenna symbols \mathbf{y} , an estimated channel \mathbf{H} and estimated noise variance σ_n^2 , our model can use them to accommodate a broad range of practical applications.

In *quantization* mode our algorithm is compatible with any external module that estimates the log-likelihood ratios (e.g., the ZF-SIC algorithm). The vector of values corresponding to a channel use is fed to the encoder f_Q and the result is quantized with the operator \mathcal{Q} . The obtained bit-vector is stored for future use or efficiently transmitted over a relay channel, after which the recovered LLR vector is obtained with g .

In *estimation* mode the algorithm directly passes \mathbf{y} , \mathbf{H} and σ_n through the estimation encoder and the decoder without quantizing the latent representation. This produces the estimated LLR vector $\tilde{\mathbf{\Lambda}}$. In *joint estimation and quantization* mode, we have the option of quantizing the latent representation obtained with the estimation encoder. Since the latent space is only trained in the first stage we thus enjoy the benefit of a robust reconstruction after applying a quantization operator. This mode also serves to evaluate the quality of the representation learned by the estimation encoder in the second stage.

C. Importance of Two-Stage Training

To highlight the importance of quantization pre-training, we investigate the difference in performance against a baseline single-stage training method. We note that this method has been successfully applied SISO log-likelihood ratio estimation [12] in the form of a very simple two-layer perceptron. To perform a calibrated comparison, we use exactly the same architecture in

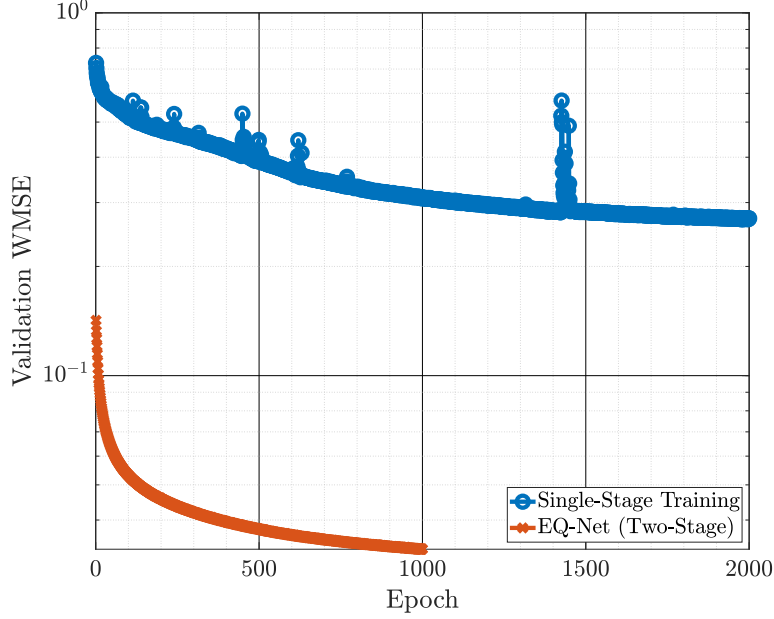
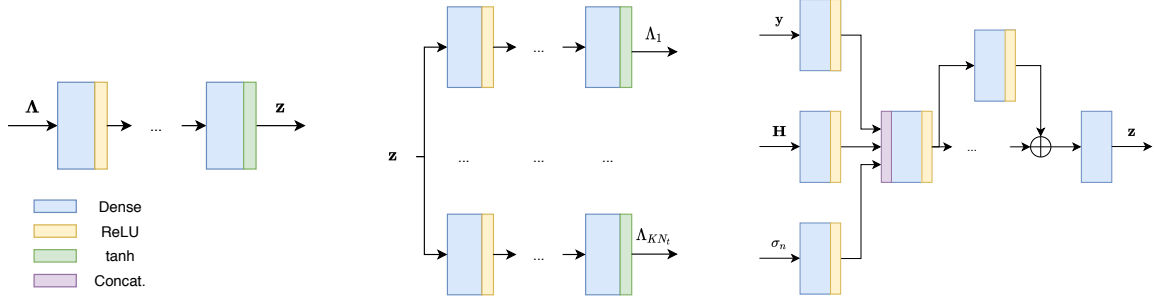


Fig. 3. Validation loss during training progression for EQ-Net and a baseline approach that jointly trains the estimation encoder and the decoder. In both cases, the networks have the same architecture and initial weights. The baseline is jointly trained for twice as long, but even this cannot compensate for the poor convergence caused by the latent bottleneck.

both cases: the estimation encoder is a residual network, while the shared decoder is a branched architecture. For the baseline, we train the two networks jointly for a total of 2000 epochs, with the learning rate divided by a factor of two if the validation loss does not improve for 100 consecutive epochs. For our proposed approach, each stage is trained for the same number of 1000 epochs, to achieve a fair comparison. Furthermore, we increase the starting learning rate for the joint approach to compensate for the untrained latent representation.

Fig. 3 plots the evolution of the validation loss across the training period for both methods in a 2-by-2, 64-QAM scenario under i.i.d. Rayleigh fading. This highlights the superior performance of the proposed method: baseline single-stage (joint) training is inefficient and falls into a local minima, whereas the two-stage method converges to a better solution, even though each component (encoder and decoder) is separately trained for *half* the time of joint training. Note that for SISO scenarios (more broadly, MIMO channels with orthogonal channels), as highlighted in [12], the ML solution in (2) admits a high-fidelity piecewise linear approximation in the form of the max-log-MAP estimator, in which case a two-layer neural network can be easily trained to match the performance of our approach. This is owed to the particular structure of QAM with Gray coding, but this observation does not straightforwardly extend to high-dimensional



(a) Quantization encoder f_Q with a simple and shallow MLP structure. (b) Shared decoder g with a branched architecture. (c) Input layers and one residual block of the estimation encoder f_E . Multiple residual blocks can be concatenated to form f_E .

Fig. 4. Internal architectures for each of the functional blocks in Fig. 2 implemented as deep neural networks.

channels.

V. EXPERIMENTAL RESULTS

A. Implementation Details

The models f_Q , f_E and g are all comprised of deep neural networks, sharing a common design principle: reducing the end-to-end latency as much as possible to make our architecture suitable for real-time deployments. The most straightforward way of achieving this goal is by limiting the depth of all networks while potentially increasing their width, in order to leverage parallel processing capabilities. A detailed block diagram of the models is shown in Fig. 4. All models use the ReLU activation function across all hidden layers. Across training and testing, the LLR vector is pre-processed by converting it to the hyperbolic domain via the element-wise function $f(x) = \tanh(x/2)$. For scenarios with $N_t = 2$ we use a single residual block in the encoder, while for $N_t = 4$ we use three blocks to compensate for the higher-dimensional nature of the problem.

For training, we use the Adam optimizer [18] with a batch size of 32768 samples, a learning rate of 0.001 and default Tensorflow parameters for both stages. Training data consists of pre-generated LLR vectors coming from 10000 packets at six logarithmically spaced SNR values, such that the block error rate of ML estimation is between 1 and 0.0001, where SNR is defined as $\frac{\mathbb{E}[\|\mathbf{H}\|_F^2]}{\sigma_n^2}$. We use a low-density parity check (LDPC) code of size (324, 648), leading to a total of 2.7 million training samples for a 2-by-2 64-QAM scenario and slightly less for 4-by-4 16-QAM. We reserve 20% of these samples as validation data. Testing is performed with the

same channel coding scheme across a wider array of SNR values. Our scheme does not suffer a performance loss if tested on other codes (e.g., polar), but we omit these results for brevity.

The quantization encoder f_Q has a simple structure as a fully-connected multi-layer perceptron (MLP) with six hidden layers, each with a width of $4N_tK$, and an output layer of size $d_{\text{ZF-SIC}} = 3N_t$. Note that the width scales with modulation order but the depth is fixed, allowing us to increase the expressive power of the network without sacrificing latency in more difficult high-order modulation scenarios.

The estimation encoder f_E takes as input the triplet $(\mathbf{y}, \mathbf{H}, \sigma_n)$ and first passes their flattened, real-valued (obtained by concatenating the flattened real and imaginary parts in a single real-valued vector) versions through a separate dense layer for each channel, followed by a concatenation operation. This is analogous to an early feature fusion strategy, since the three input signals have different physical dimensions and interpretations. The building block of the estimation encoder contains an additional six hidden layers with residual connections between them, as shown in Fig. 4c. The reason for not including these connections in the quantization encoder is empirical and based on the sufficiently good performance offered by f_Q without them.

The shared decoder g uses the same branched architecture described in [14]: the latent representation is separately processed on $N_t \times K$ parallel MLPs, each with six hidden layers. This architecture effectively learns a separate decoding function for each individual entry in the log-likelihood ratio vector, while still taking the entire latent representation as input.

To discretize the latent representation during testing, where gradients are no longer needed, we learn a factorized quantization codebook by separately applying a quantization function to each dimension of the latent space. We use the same data-based approach as [14] and train a k-means++ [19] scalar quantizer after f_Q and g have been trained with the L_2 distance in the latent space. Note that this is not the only possible choice here, but in practice we find little benefit to training a vector quantizer owing to the non-convex nature of the problem.

B. Estimation Performance

The number of residual blocks used in the encoder f_E serves as a simple adjustment between the latency and performance of EQ-Net. We train two variants: EQ-Net-L (a low-latency architecture with one residual block) and EQ-Net-P (a high-performance architecture with three residual blocks). We compare our method with two state-of-the-art approaches that involve deep learning, as well as the baseline ZF-SIC detector and the optimal ML algorithm. The two deep

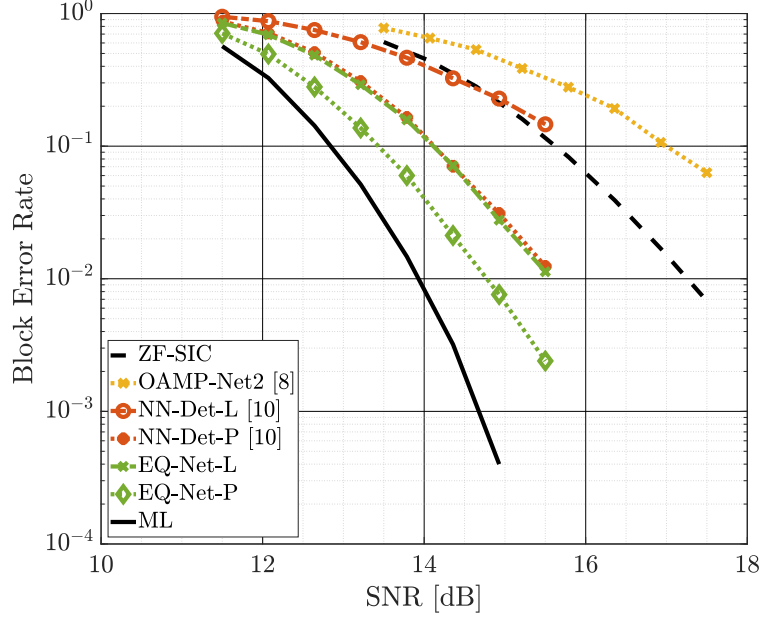


Fig. 5. Estimation (MIMO detection) performance of EQ-Net versus state-of-the-art approaches in a 2-by-2, 64-QAM Rayleigh fading and LDPC-coded scenario. Table I further compares the end-to-end latency of all methods.

learning baselines are the scheme in [10], which we further refer to as NN-Det for brevity, and the OAMP-Net2 approach in [8].

We implement both baselines in TensorFlow and follow the original design principles as closely as possible, while searching for their best hyperparameters. For NN-Det, we use exactly the same per-iteration structure as [10] with hidden sizes of 250 and 150. We reach the same conclusion as [10] regarding the training regime: training at a sufficiently large SNR value is critical for a good solution that can be used across the entire range. We find a learning rate of 10^{-4} and batch size of 2048 work best when trained at an SNR of 20 dB for a 2-by-2 64-QAM scenario. To compensate for training at a single SNR points, we use five times more training data (50000 packets). For 2-by-2 64-QAM we train two variants of NN-Det: NN-Det-P (4 unfolded blocks) with the same end-to-end performance as our proposed method and NN-Det-L (3 unfolded blocks) which trades off some of the performance for lower end-to-end latency. We find that further decreasing the number of blocks drastically reduces performance. For 4-by-4 16-QAM, we train a single NN-Det model with 10 unfolded blocks.

For OAMP-Net2, we only use the detector part with trainable step sizes and do not perform channel estimation, instead relying on exact CSI. Our own implementation confirms the authors'

TABLE I
LATENCY BENCHMARKS OF EVALUATED SOFT-OUTPUT MIMO DETECTION ALGORITHMS FOR A 2-BY-2 64-QAM
SCENARIO. ALL VALUES EXPRESSED IN MILLISECONDS. B REPRESENTS THE BATCH SIZE DURING INFERENCE.

	EQ-Net-L	EQ-Net-P	NN-Det-L	NN-Det-P	OAMP-Net2
Latency CPU, $B = 256$	3.018	5.142	5.144	6.476	3.939
Latency CPU, $B = 16$	1.767	2.292	2.565	3.073	2.376
Latency CPU, $B = 1$	1.511	1.903	2.269	2.689	2.125
Latency GPU, $B = 8192$	6.523	8.767	12.610	15.914	25.940

conclusion that increasing the number of unfolds past six does not bring any substantial benefit, thus we use the values of 4 and 6 for our two MIMO scenarios, respectively. We learn separate step sizes for each particular SNR value and find that a learning rate of 10^{-4} and batch size of 100 lead to the the most stable learning behaviour. At test time, for both NN-Det and OAMP-Net2 we form the log-likelihood ratios by summing all the corresponding symbol probabilities for the terms in (2), since these methods output symbol probabilities.

We measure the end-to-end latency by implementing all methods as compact computational graphs in Keras + Tensorflow 1.15 and only timing the average duration of 10000 calls of the `predict` method (after a number of warm-up rounds). We time using the `timeit` Python module. The CPU is an Intel i9-9900x with 10 cores running at 3.5 GHz and the GPU is an NVIDIA RTX 2080Ti.

We find that both variants of EQ-Net surpass the prior work in performance with a gain of more than 2 dB and in latency with at least a 60% speed up. Fig. 5 and 6 plot the performance of the considered algorithms, while Tables I and II show the corresponding latency. For the 64-QAM scenario, the low latency version of EQ-Net achieves the same performance as the high-performance (and latency) version of NN-Det. This is better highlighted in Fig. 6, where we only compare EQ-Net-L with NN-Det-P and reach the same conclusion. This result highlights the benefits of pre-training the compressed feature space: while the number of learnable parameters in EQ-Net and NN-Det are approximately the same — in the order of hundreds of thousands

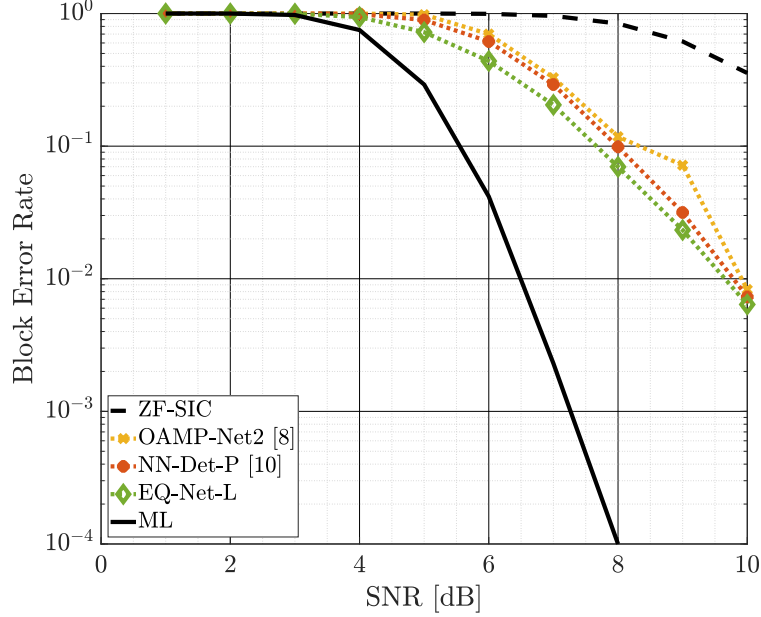


Fig. 6. End-to-end estimation performance of proposed algorithms against state-of-the-art approaches in a 4-by-4, 16-QAM Rayleigh fading scenario. Table II further compares the end-to-end latency of all methods.

TABLE II
LATENCY BENCHMARKS OF EVALUATED SOFT-OUTPUT MIMO DETECTION ALGORITHMS FOR A 4-BY-4 16-QAM SCENARIO. ALL VALUES EXPRESSED IN MILLISECONDS. B REPRESENTS THE BATCH SIZE DURING INFERENCE.

	EQ-Net-L	NN-Det-P	OAMP-Net2
Latency CPU, $B = 256$	2.095	16.235	9.189
Latency CPU, $B = 16$	1.711	5.957	3.437
Latency CPU, $B = 1$	1.561	5.113	3.154
Latency GPU, $B = 8192$	6.523	29.310	35.727

— the estimator learned by EQ-Net is much more efficient in using these parameters.

The reduced latency can be attributed to the fact that the baseline approaches require additional linear algebra computations which are sequential in nature, such as matrix inversion and conjugate-multiply. In contrast, our approach does not involve any of these steps: we take in

the raw inputs and directly output the LLR vector. This fact becomes even more apparent when the algorithms are run on specialized inference hardware (i.e., GPUs). The last line in both tables highlights the increasing latency gap when the algorithm is deployed in a scenario with a massive number of users, where a single base station (or cloud computing device) performs computations in large batches.

The performance of EQ-Net can be further explained via the *information bottleneck* method [4]. By learning a feature space that compresses \mathbf{z} to a minimal size that does not introduce large distortions, EQ-Net learns how to extract only the most relevant features of the LLR vector, leading in turn to efficient estimation. As Fig. 5 and 6 show, the choice of $\dim(\mathbf{z}) = d_{\text{ZF-SIC}}$ accurately captures this behaviour. This is in stark contrast to prior methods that use model-based approaches for detection and have to pay a price in increased latency — in the form of iterations or depth — for increased performance.

C. Quantization Performance

For the quantization task, we investigate the performance of EQ-Net against the maximum mutual information quantizer in [13] and the deep learning based scheme in [14], which is designed for SISO scenarios. To extend this to a MIMO scenario, we simply split the LLR vector into sub-vectors along the transmitted stream and quantize each of them separately. This serves as a strong baseline that also reveals the gain obtained by considering redundancy across the spatial dimension. For our approach, we train a separate k-means++ quantizer with 64 levels for each scalar dimension of the latent space, thus requiring six bits of storage for each latent component. For a 2-by-2 64-QAM scenario, this amounts to compressing the entire vector of 12 LLR values down to a 36-bit codeword, leading to an effective compression ratio of three bits per LLR.

Compared to [14], EQ-Net achieves a 16% compression gain with the same end-to-end performance, whereas compared to [13] EQ-Net boosts the performance of the system 0.65 dB while using same compression ratio. The simulation results are plotted in Fig. 7, which demonstrates that our approach is superior to both baseline methods and can efficiently compress the LLR vector using the rate with a minimal performance loss. The difference in performance when compared to [14] highlights the importance of jointly learning a feature space across the spatial dimensions of a MIMO channels. Even though the compression ratio of EQ-Net is the

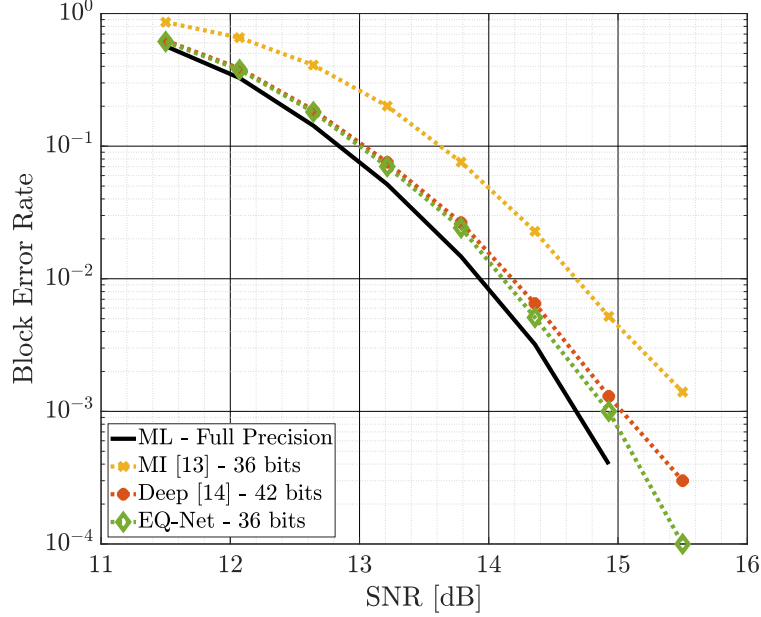


Fig. 7. Quantization performance of EQ-Net evaluated against state-of-the-art methods in a 2-by-2, 64-QAM, i.i.d. Rayleigh fading and LDPC-coded scenario.

same as [14], Fig. 7 shows that compressing the entire Λ leads to more a more robust feature space when numerical quantization is applied.

EQ-Net also has the advantage of supporting a non-uniform quantization rate. For example, if five bits are used to store each latent component then the entire LLR vector can be stored using 30 values with an effective 2.5 bits per LLR. In contrast, classical compression methods that are applied to each LLR position individually would have to use an imbalanced compression scheme to achieve fractional rates, potentially leading to increased error floors in the system performance.

VI. ROBUSTNESS TO DISTRIBUTIONAL SHIFTS

All the data-driven approaches so far have been tested on the same distributions as the ones they were trained on. Practical scenarios may, however, involve either severe distributional shifts (e.g., completely different fading models) or faced with imperfect knowledge. For LLR estimation and quantization, the most fragile part of the system is given from the CSI matrix \mathbf{H} and any distributional mismatch that may occur. To evaluate the robustness of our approach, we consider models trained on \mathbf{H} matrices from an i.i.d. Rayleigh fading model and tested — without *any* further adjustments or fine-tuning — on realizations of the CDL-A channel model adopted by the

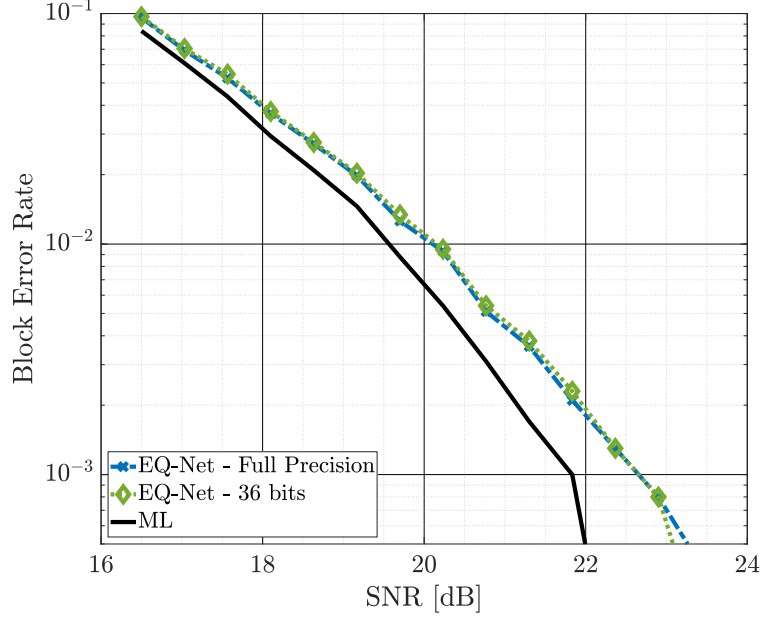


Fig. 8. Quantization performance of EQ-Net under a severe distributional shift induced by training on an i.i.d. Rayleigh fading channel and testing on the 5G-NR CDL-A MIMO channel model for a 2-by-2 64-QAM LDPC-coded scenario.

5G-NR specifications [20]. This is a realistic model that has a larger degree of spatial correlation than the Rayleigh model and is driven by physical propagation laws.

Fig. 8 shows the quantization performance under this shift in a 2-by-2 64-QAM scenario. While a performance gap of around 1 dB appears between our compression method (that compresses to a low-dimensional space, but does not quantize) and the ML solution, the scheme is overall extremely robust and does not exhibit any error floors. Furthermore, when quantizing down to the same ratio of 3 bits/LLR, there is virtually no performance loss incurred.

Fig. 9 further investigates the estimation performance under the same shift and reveals a much higher degree of robustness than the baseline NN-Det-P and retaining a performance close to that of the ZF-SIC algorithm. For the remainder of this section, for estimation tasks we always compare our low-latency approach (EQ-Net-L) with the high-performance baseline (NN-Det-P). While the two methods started from a very similar same end-to-end performance, as shown in Fig. 5, EQ-Net can avoid a severe error floor. We attribute this robustness to the information bottleneck applied during training, as well as the particular expression of the WMSE loss used during training. Eq. 7 increases the weight of uncertain LLR values, which are more likely to occur in scenarios with ill-conditioned channels, such as those from the CDL-A model. Overall,

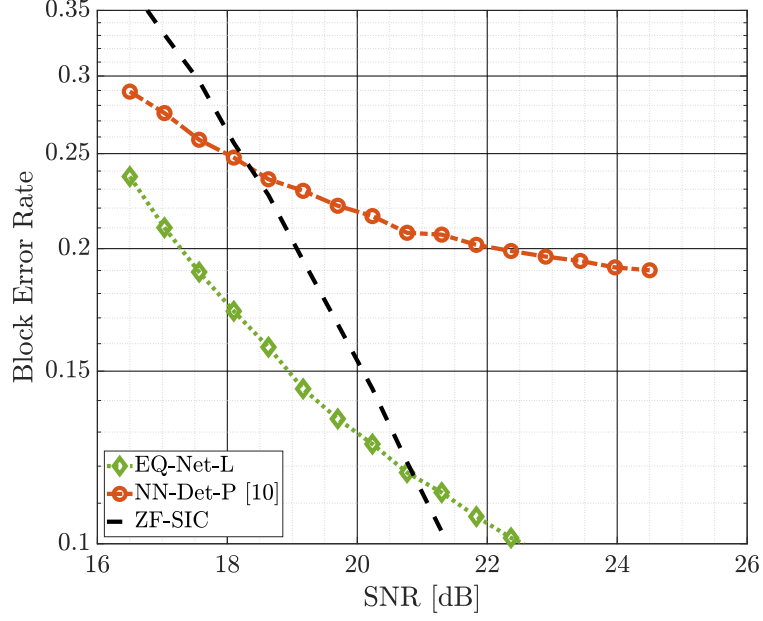


Fig. 9. Estimation performance of EQ-Net and the similarly performing NN-Det-P [10] under severe distributional shift induced by training on an i.i.d. Rayleigh fading channel and testing on the 5G-NR CDL-A MIMO channel model for a 2-by-2 64-QAM LDPC-coded scenario.

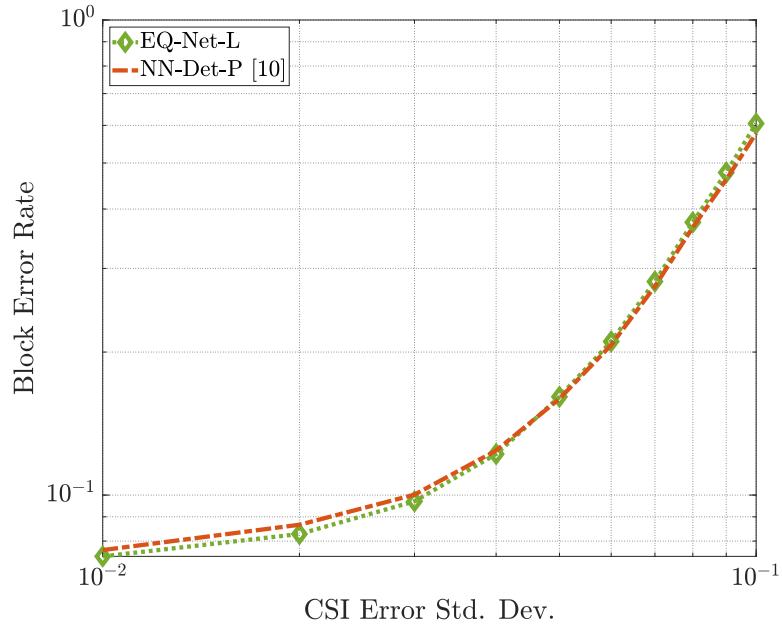


Fig. 10. Estimator robustness of EQ-Net and the similarly performing NN-Det-P [10] under imperfect CSI for a 2-by-2 64-QAM LDPC-coded scenario. For better visualization, we only plot the evolution of block error rate at an SNR value of 14.35 dB as the CSI error increases.

our result highlights the potential of *robust* feature learning for LLR estimation versus model-based approaches, which ultimately still rely on a pre-specified or estimated distribution.

Finally, we also investigate the performance of our approach in the case of CSI estimation impairments. For this we use a corrupted version of an \mathbf{H} coming from an i.i.d. Rayleigh fading model as $\hat{\mathbf{H}} = \mathbf{H} + \mathbf{N}$, where \mathbf{N} is an i.i.d. Gaussian noise with covariance matrix $\sigma_{CSI}\mathbf{I}$. This models impairments coming from the channel estimation module. Fig. 10 shows that our algorithm is robust to these impairments as well, remaining on par with the NN-Det-P algorithm and still benefiting from the much lower end-to-end latency in Table I.

VII. CONCLUSIONS

In this paper we have proposed a deep learning framework that jointly solves the tasks of log-likelihood ratio estimation and quantization in a MIMO scenario. We have used theoretical results on classical algorithms to design the dimension of a learned feature space. Our approach has been shown to be practical in terms of latency and is compatible with any MIMO system, such as the MIMO-OFDM used in 5G scenarios, relaying scenarios, or distributed over-the-air communication systems — such as the ones used in federated learning — which would benefit from both quantization and estimation gains. Throughout evaluation, our approach has shown superior performance, exceptional distributional robustness and on-par impairment robustness to state-of-the-art estimation methods. We find these results encouraging, since our method could easily be extended to account for perturbations during training. Another promising direction for future work is removing the requirement of training a separate model for each MIMO configuration and leveraging flexible deep learning architecture to learn truly universal algorithms for LLR processing.

REFERENCES

- [1] A. Zappone, M. Di Renzo, and M. Debbah, “Wireless networks design in the era of deep learning: Model-based, ai-based, or both?” *IEEE Transactions on Communications*, vol. 67, no. 10, pp. 7331–7376, 2019.
- [2] M. Bennis, M. Debbah, and H. V. Poor, “Ultrareliable and low-latency wireless communication: Tail, risk, and scale,” *Proceedings of the IEEE*, vol. 106, no. 10, pp. 1834–1853, 2018.
- [3] P. Kairouz, H. B. McMahan, B. Avent, A. Bellet, M. Bennis, A. N. Bhagoji, K. Bonawitz, Z. Charles, G. Cormode, R. Cummings *et al.*, “Advances and open problems in federated learning,” *arXiv preprint arXiv:1912.04977*, 2019.
- [4] N. Tishby, F. C. Pereira, and W. Bialek, “The information bottleneck method,” *arXiv preprint physics/0004057*, 2000.
- [5] A. A. Alemi, I. Fischer, J. V. Dillon, and K. Murphy, “Deep variational information bottleneck,” *arXiv preprint arXiv:1612.00410*, 2016.

- [6] P. W. Wolniansky, G. J. Foschini, G. D. Golden, and R. A. Valenzuela, “V-BLAST: An architecture for realizing very high data rates over the rich-scattering wireless channel,” in *Proc. URSI Intl. Symp. on Signals, Syst., and Electron.*, 1998, pp. 295–300.
- [7] C. Studer, A. Burg, and H. Bolcskei, “Soft-output sphere decoding: Algorithms and VLSI implementation,” *IEEE JSAC*, vol. 26, no. 2, pp. 290–300, 2008.
- [8] H. He, C.-K. Wen, S. Jin, and G. Y. Li, “Model-driven deep learning for joint MIMO channel estimation and signal detection,” *arXiv preprint arXiv:1907.09439*, 2019.
- [9] J. Ma and L. Ping, “Orthogonal AMP,” *IEEE Access*, vol. 5, pp. 2020–2033, 2017.
- [10] O. Sholev, H. H. Permuter, E. Ben-Dror, and W. Liang, “Neural network MIMO detection for coded wireless communication with impairments,” in *Proc. IEEE Wireless Commun. Netwk. Conf.*, 2020, pp. 1–8.
- [11] N. Shlezinger, N. Farsad, Y. C. Eldar, and A. J. Goldsmith, “ViterbiNet: A deep learning based Viterbi algorithm for symbol detection,” *IEEE Trans. Wireless Commun.*, vol. 19, no. 5, pp. 3319–3331, 2020.
- [12] O. Shental and J. Hoydis, “Machine LLRning: Learning to softly demodulate,” in *Proc. IEEE Global Commun. Conf. Workshops*, 2019, pp. 1–7.
- [13] A. Winkelbauer and G. Matz, “On quantization of log-likelihood ratios for maximum mutual information,” in *Proc. IEEE Intl. Workshop on Signal Proc. Adv. in Wireless Commun.*, 2015, pp. 316–320.
- [14] M. Arvinte, S. Vishwanath, and A. H. Tewfik, “Deep learning-based quantization of L-values for Gray-coded modulation,” in *Proc. IEEE Global Commun. Conf. Workshops*, 2019, pp. 1–6.
- [15] R. T. Kobayashi and T. Abrão, “Ordered mmse-sic via sorted qr decomposition in ill conditioned large-scale mimo channels,” *Telecommunication systems*, vol. 63, no. 2, pp. 335–346, 2016.
- [16] D. Tse and P. Viswanath, *Fundamentals of Wireless Communication*. Cambridge University Press, 2005.
- [17] G. Hinton, O. Vinyals, and J. Dean, “Distilling the knowledge in a neural network,” *arXiv preprint arXiv:1503.02531*, 2015.
- [18] D. P. Kingma and J. Ba, “Adam: A method for stochastic optimization,” *arXiv preprint arXiv:1412.6980*, 2014.
- [19] D. Arthur and S. Vassilvitskii, “k-means++: The advantages of careful seeding,” Tech. Rep., 2006.
- [20] *Study on channel model for frequency spectrum above 6 GHz*, 3GPP, 2019.

APPENDIX A

PROOF OF THEOREM 1

We prove this by induction. Consider the form of (1) after left-side multiplication with \mathbf{Q}^H as

$$\tilde{\mathbf{y}} = \mathbf{Q}^H \mathbf{y} = \mathbf{R} \mathbf{x} + \mathbf{Q}^H \mathbf{n} = \mathbf{R} \mathbf{x} + \hat{\mathbf{n}}.$$

Assuming that \mathbf{n} is i.i.d. Gaussian, then $\hat{\mathbf{n}}$ is i.i.d. Gaussian as well due to the orthogonal columns of \mathbf{Q} . Using that \mathbf{R} is upper-triangular and that Algorithm 1 uses only the last element of $\hat{\mathbf{y}}$, we have the equation

$$\hat{y}_{N_t} = r_{N_t, N_t} x_{N_t} + \hat{n}_{N_t}.$$

This leads to the closed-form expression of the K LLR values corresponding to the N_t -th symbol as

$$\Lambda_{k,N_t} = \log \frac{\sum_{x_j, b=1} \exp -|\hat{y}_{N_t} - r_{N_t,N_t} x_j|^2}{\sum_{x_j, b=0} \exp -|\hat{y}_{N_t} - r_{N_t,N_t} x_j|^2}.$$

Then, the previous equation also serves as a function $g(\hat{y}_{N_t}, r_{N_t,N_t}) = \Lambda_{:,N_t}$. Given that \hat{y}_{N_t} is a complex scalar and r_{N_t,N_t} is a real scalar, it follows that the LLR vector corresponding to the last spatial stream can be exactly represented by a three dimensional real vector. This proves the case $N_t = 1$. The equation for estimating the LLR values corresponding to the K -th symbol, given the previous $K - 1$ estimates is then

$$\hat{y}_K = r_{K,K} x_K + \sum_{k=1, \dots, K-1} r_{K,K-k} x_{K-k} + \hat{n}_{N_t}.$$

Letting $\hat{t}_K = \hat{y}_K - \sum_{k=1, \dots, K-1} r_{K,K-k} x_{K-k}$, we have the compact equation

$$\hat{t}_K = r_{K,K} x_K + \hat{n}_{N_t}.$$

It follows that, given estimates for the previous $K - 1$ symbols, the LLR values of the K -th symbol can be exactly represented by a vector with three real values, regardless of modulation order. Thus, by induction, $d_{\text{ZF-SIC}} = 3N_t$.

APPENDIX B

PROOF OF THEOREM 2

We prove this by inspecting the form of (1) after left-side multiplication with \mathbf{Q}^H as

$$\tilde{\mathbf{y}} = \mathbf{Q}^H \mathbf{y} = \mathbf{R} \mathbf{x} + \mathbf{Q}^H \mathbf{n} = \mathbf{R} \mathbf{x} + \hat{\mathbf{n}}.$$

Then, there exists a function such that $g(\mathbf{y}, \mathbf{R}) = \Lambda$, given exactly by (3). Since \mathbf{y} is a complex-valued vector of length N_t and \mathbf{R} is a complex-valued upper triangular matrix of size $N_t \times N_t$ with a real-valued diagonal, we immediately have that

$$d_{\text{ML}} = 2N_t + N_t + 2 \frac{(N_t - 1)N_t}{2} = N_t(N_t + 2).$$

The first term corresponds to \mathbf{y} , the second to the real-valued diagonal of \mathbf{R} and the third to the off-diagonal complex-valued terms in \mathbf{R} .